REGIONAL SEISMIC AMPLITUDE MODELING AND TOMOGRAPHY FOR EARTHQUAKE-EXPLOSION DISCRIMINATION

William R. Walter, Michael E. Pasyanos, Eric Matzel, Rengin Gök, Jerry J. Sweeney, Sean R. Ford and Arthur J. Rodgers

Lawrence Livermore National Laboratory

Sponsored by National Nuclear Security Administration

Contract No. DE-AC52-07NA27344

ABSTRACT

We continue exploring methodologies to improve earthquake-explosion discrimination using regional amplitude ratios such as *P/S* in a variety of frequency bands. Empirically, we demonstrate that such ratios separate explosions from earthquakes, using closely located pairs of earthquakes and explosions recorded on common, publicly available stations at test sites around the world (e.g., Nevada, Novaya Zemlya, Semipalatinsk, Lop Nor, India, Pakistan, and North Korea). We are also examining if there is any relationship between the observed *P/S* and the point source variability revealed by longer period full waveform modeling (e.g., Ford et al., 2008). For example, regional waveform modeling shows strong tectonic release from the May 1998 India test, in contrast with very little tectonic release in the October 2006 North Korea test, but the *P/S* discrimination behavior appears similar in both events using the limited regional data available.

While regional amplitude ratios such as *P/S* can separate events in close proximity, it is also empirically well known that path effects can greatly distort observed amplitudes and make earthquakes appear very explosion-like. Previously we have shown that the Magnitude Distance Amplitude Correction (MDAC) technique (Walter and Taylor, 2001) can account for simple 1-D attenuation and geometrical spreading corrections, as well as magnitude and site effects. However, in some regions, 1-D path corrections are a poor approximation, and we need to develop 2-D path corrections. Here we demonstrate a new 2-D attenuation tomography technique using the MDAC earthquake source model applied to a set of events and stations in both the Middle East and the Yellow Sea Korean Peninsula regions. We believe this new 2-D MDAC tomography has the potential to greatly improve earthquake-explosion discrimination, particularly in tectonically complex regions such as the Middle East.

Report Documentation Page

Form Approved
OMB No. 0704-0188

1. REPORT DATE	2. REPORT TYPE	3. DATES COVERED
SEP 2008		**00-00-2008 to 00-00-2008**

4. TITLE AND SUBTITLE	5a. CONTRACT NUMBER
Regional Seismic Amplitude Modeling and Tomography for Earthquake-Explosion Discrimination	5b. GRANT NUMBER
	5c. PROGRAM ELEMENT NUMBER
6. AUTHOR(S)	5d. PROJECT NUMBER
	5e. TASK NUMBER
	5f. WORK UNIT NUMBER
7. PERFORMING ORGANIZATION NAME(S) AND ADDRESS(ES) **Lawrence Livermore National Laboratory,PO Box 808,Livermore,CA,94551-0808**	8. PERFORMING ORGANIZATION REPORT NUMBER
9. SPONSORING/MONITORING AGENCY NAME(S) AND ADDRESS(ES)	10. SPONSOR/MONITOR'S ACRONYM(S)
	11. SPONSOR/MONITOR'S REPORT NUMBER(S)

12. DISTRIBUTION/AVAILABILITY STATEMENT
Approved for public release; distribution unlimited

13. SUPPLEMENTARY NOTES
Proceedings of the 30th Monitoring Research Review: Ground-Based Nuclear Explosion Monitoring Technologies, 23-25 Sep 2008, Portsmouth, VA sponsored by the National Nuclear Security Administration (NNSA) and the Air Force Research Laboratory (AFRL)

14. ABSTRACT
see report

15. SUBJECT TERMS

16. SECURITY CLASSIFICATION OF:			17. LIMITATION OF ABSTRACT	18. NUMBER OF PAGES	19a. NAME OF RESPONSIBLE PERSON
a. REPORT	b. ABSTRACT	c. THIS PAGE			
unclassified	**unclassified**	**unclassified**	**Same as Report (SAR)**	**10**	

OBJECTIVES

Monitoring the world for potential nuclear explosions requires characterizing seismic events and discriminating between natural and man-made seismic events, such as earthquakes and mining activities, and nuclear weapons testing. We continue developing, testing, and refining size-, distance-, and location-based regional seismic amplitude corrections to facilitate the comparison of all events that are recorded at a particular seismic station. These corrections, calibrated for each station, reduce amplitude measurement scatter and improve discrimination performance. We test the methods on well-known (ground truth) datasets in the U.S. and then apply them to the uncalibrated stations in Eurasia, Africa, and other regions of interest to improve underground nuclear test monitoring capability.

RESEARCH ACCOMPLISHED

As part of the overall National Nuclear Security Administration Ground-Based Nuclear Explosion Monitoring Research and Development (GNEMRD) program, we continue to pursue a comprehensive research effort to improve our capabilities to seismically characterize and discriminate underground nuclear tests from other natural and man-made sources of seismicity. To reduce the monitoring magnitude threshold, we make use of local and regional body and surface wave data to calibrate each seismic station. Our goals are to reduce the variance and improve the separation between explosions and other event populations by accounting for the effects of propagation and differential source size and by optimizing the types and combinations of amplitude measurements used.

Empirical *P/S* Observations

Empirical observations have shown clear differences between earthquake and explosion *P/S* amplitude ratios that can be exploited for nuclear explosion monitoring. These differences became apparent with the advent of widespread digital seismometry in the late 1980s and early 1990s, when a large number of different researchers found that at high frequencies, greater than around 2-4 Hz, the regional *P/S* amplitude ratios consistently discriminated explosions from earthquakes (e.g., Dysart and Pulli, 1987; Baumgardt and Young, 1990; Kim et al., 1993; Walter et al., 1995; Taylor, 1996; Hartse et al., 1997; Battone et al., 2002). For example, in Figure 1 we compare an earthquake and an explosion at each of four major test sites (rows), bandpass filtered in four different frequency bands (columns). Here we use closely spaced pairs of earthquakes and explosions recorded at the same station to minimize any path and site effects, and so the observed differences come from effects in the source region. There is a relative lack of S-waves in the explosions as the frequency increases. Note also there are interesting differences between the test sites, indicating that emplacement conditions (depth, media properties, geologic and tectonic conditions, topography, etc.) play a role in relative P- and S-wave generation.

Examination of *P/S* ratios at high frequencies has now been done all over the world. As we show in Figure 2, the characteristic pattern—that explosions have larger relative P-wave amplitudes than S-wave amplitudes—appears to hold everywhere, provided that we filter the data at a high enough frequency and that we compare events with very similar paths. One example in Figure 2 is the announced nuclear test by North Korea on October 9, 2006. In this case, the nearest earthquakes for comparison are around 100 km away, but we can bracket the test with earthquakes and clearly see that it is deficient in high frequency S-wave energy. This example shows the importance of accounting for path, as the S-wave energy in this case is partitioned into both Sn and Lg phases. The path of the recorded seismic energy crosses the Sea of Japan, a region of oceanic crust where Lg does not efficiently propagate. On can see that this earthquake, with a greater proportion of its path in the Sea of Japan, has stronger Sn than the other. It is important to correct for path effects and to consider *P/S* ratios for all the observable regional phases and avoid cases where one of the earthquake S-wave phases is attenuated to below the level of the noise and it appears explosion-like simply due to the path effects.

When similar-sized earthquakes and explosions are nearly co-located, we can understand the observed seismic contrasts, such as the relative P-to-S wave excitation, in terms of depth, material property, focal mechanism, and source time function differences. However, it is well known that path propagation effects (e.g., attenuation, blockage) and source scaling effects (e.g., corner frequency scaling with magnitude) can make earthquakes look like explosions and vice versa. We developed the MDAC technique (Walter and Taylor, 2001) to account for these

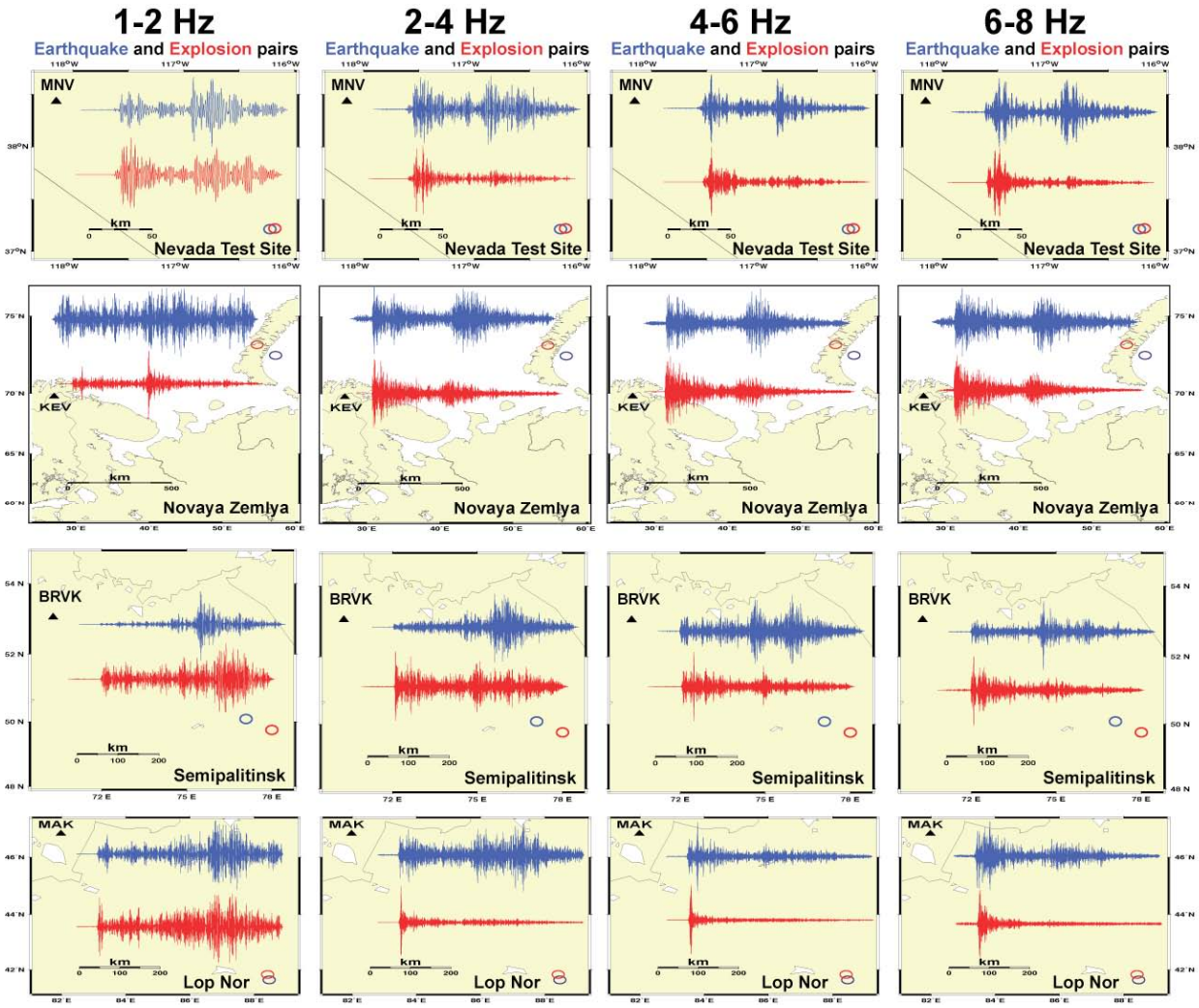

Figure 1. An earthquake and explosion pair at four different test sites: Nevada, U.S.A.; Novaya Zemlya, Russia; Semipaletinsk former U.S.S.R. now Kazakhstan; and Lop Nor, China. The seismograms are bandpass filtered at four frequency bands (columns) illustrating significant differences in relative P and S wave amplitudes, with explosions have relatively less S-waves at higher frequencies.

effects with proper calibration. We use the earthquakes alone to determine the MDAC parameters, such as geometrical spreading, frequency dependent Q, and the average apparent stress. After calibration, the MDAC formulation provides expected spectral amplitudes as a function of phase, frequency, magnitude and distance. These can then be subtracted from the actual observations. For earthquakes, the corrected data should exhibit a close-to-zero mean and no significant trends with magnitude and distance. Explosions should have significant non-zero mean residuals, leading to improved discrimination.

As shown in Figure 3, we applied MDAC to correct for path effects for earthquakes all around the Korean Peninsula, Yellow Sea, and northeastern China region recorded at stations MDJ and TJN, which are publicly available through data centers such as the Incorporated Research Institutions for Seismology (IRIS) and the Ocean Hemisphere Project Data Management Center (OHP-DMC). When ratios were available from both stations, they were averaged. We look at three different *P/S* ratios in four frequency bands. As Figure 3 shows, the North Korean test appears to discriminate progressively better at higher frequencies for all three types of *P/S* ratios. Due to event size, attenuation, background noise, and the need to be past the crossover distance to see Pn and Sn, not all measurements can be made for all phases and frequency bands. There are 167 earthquakes for 1–2 Hz Pg/Lg and fewer for the other ratios. In general, the number of measurements passing the signal-to-noise-ratio (SNR) thresholds (here 2 for P-waves and 1.3 for S-waves) diminishes as the frequency increases.

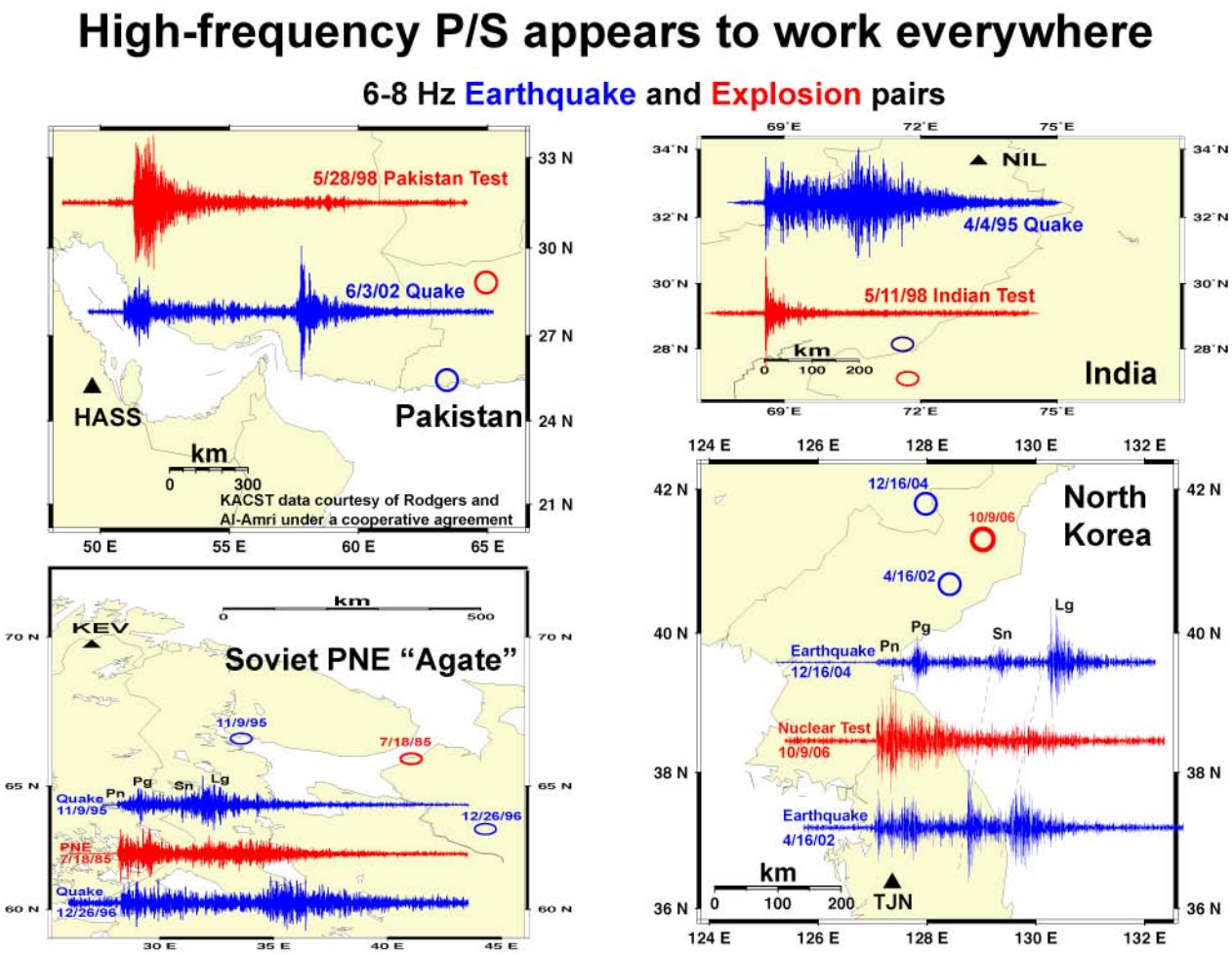

Figure 2. Four examples of 6-8 Hz filtered seismograms of explosions compared to nearby earthquakes outside the major testing areas show the characteristic difference: explosions have larger *P/S* amplitude values.

Practical considerations, such as whether we expect a new event in a particular area with a given magnitude to be detectable for a given phase and frequency, are critical for monitoring. Therefore it is good to see that there remains considerable discrimination capability in all three types of *P/S* ratios in the bands below 6–8 Hz, particularly the 2–4 and 4–6 Hz bands. As we have noted in prior MRR papers, it is possible to form multivariate combinations of ratios to enhance discrimination, and these can be tuned to optimize discrimination based on the bands you are likely to have to work with.

One type of ratio that has been considered from a practical viewpoint is the cross-spectral ratio (e.g., Taylor et al., 2002): comparing a higher frequency P-wave amplitude to a lower frequency S-wave amplitude. As shown in Figure 1 for Lop Nor or Figure 2 for India, some explosions do not have any visible S-waves at high frequency and the S-measurement is made on coda. Such explosion coda measures can work so long as one is sure a comparable-size earthquake would have produced measurable S-waves allowing discrimination. In a cross-spectral ratio, the S-wave band is chosen so that even explosion S-waves are detectable, and these have been shown to work well in some cases such as Lope Nor (e.g., Taylor et al., 2002). A complication with cross-spectral ratios occurs if the spectral decay at high frequencies is substantially different for explosions than for earthquakes: it can start to counteract the *P/S* difference and lead to poor discrimination. In Figure 4, we show an example of a 6–8 Hz Pn to 2–4 Hz Lg ratio for Nevada Test Site (NTS) data averaged over two stations, ELK and KNB. One can see that a number of the explosions do not discriminate at all. NTS explosions show a clear material property dependence (e.g., Walter et al., 1995) with explosions in weak, high-gas-porosity media having much stronger spectral decay than explosions in stronger, low-gas-porosity media when compared at the same station using the same path and site corrections, as shown in Figure 4.

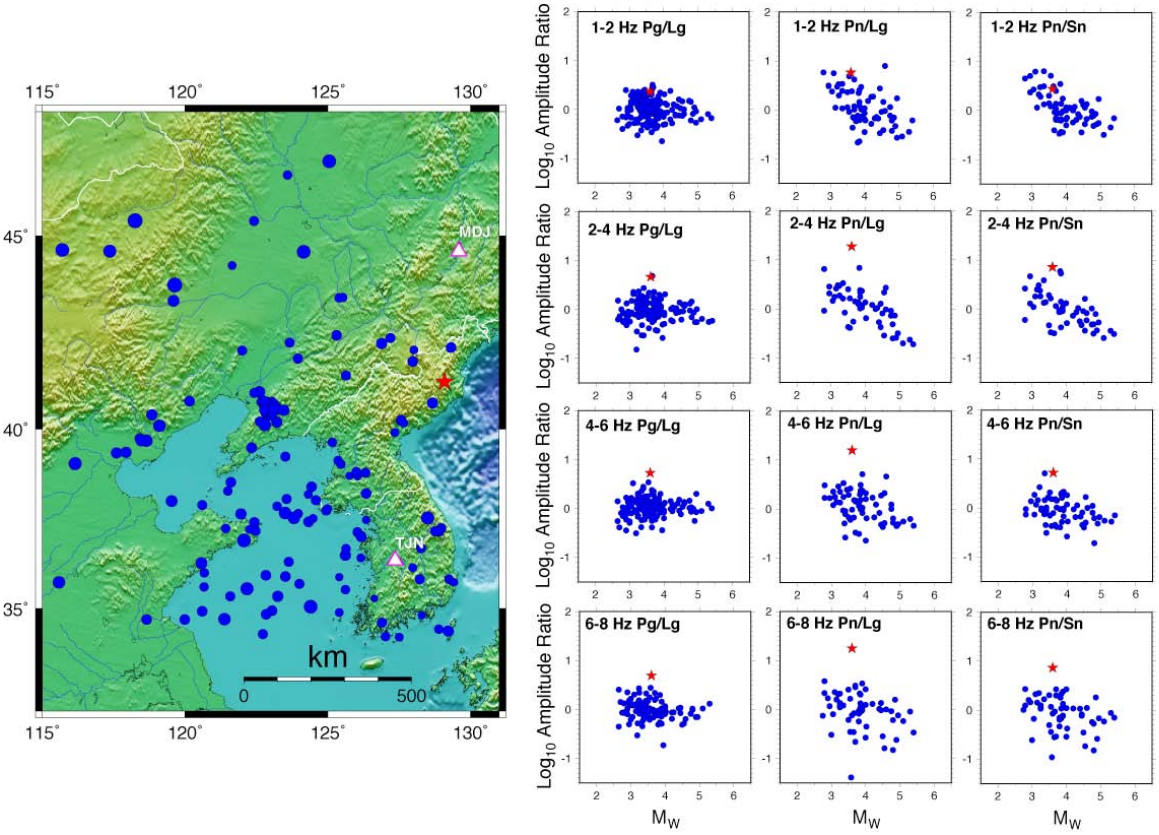

Figure 3. The map shows earthquakes (blue circles) and the October 9, 2006, North Korean nuclear test (red star) observed at seismic stations MDJ and TJN. The scatter plots show the MDAC path corrected *P/S* ratios at each station (average when both available) for three different *P/S* ratios in four different frequency bands.

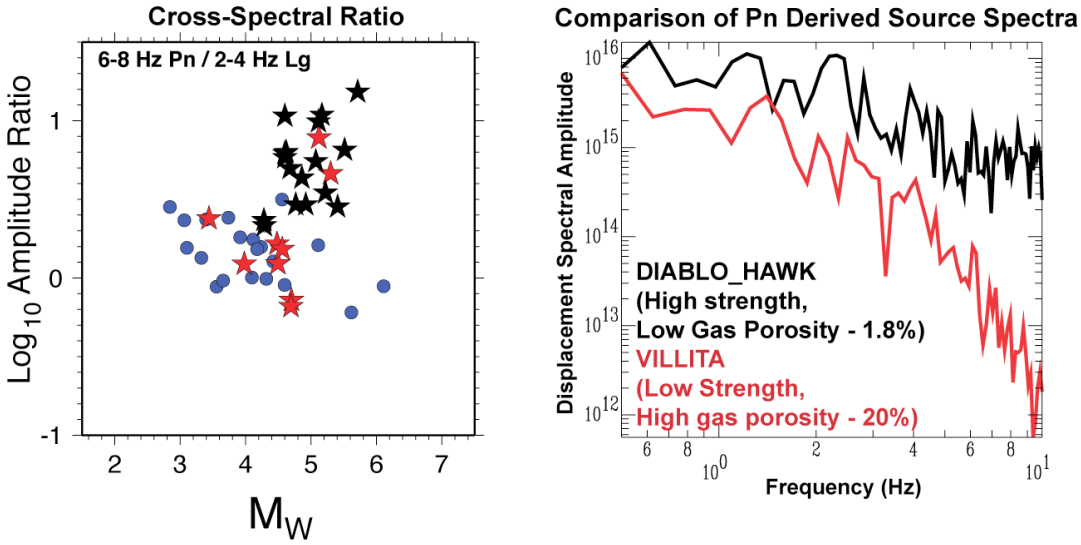

Figure 4. Left: example cross-spectral ratio for NTS area data averaged for stations ELK and KNB. Right: NTS explosions show strong material property dependence of the P and S spectra. We separate the nuclear explosions into high-strength/low-gas-porosity (black) and low-strength/high-gas-porosity (red) populations, following the criteria in Walter et al. (1995) of $\log(\rho\alpha^2) = 0.093GP + 9.4$.

In Figure 5, we show the same-frequency *P/S* ratios in different frequency bands for the ELK-KNB station averaged data color coded as in Figure 4 by media properties from Springer et al. (2002). At lower frequencies (0.5-4 Hz) there is some evidence that the material properties affect discrimination with the weak, high gas porosity events do not discriminate as well. At higher frequencies (6-16 Hz) there does not appear to be a significant difference though the dataset starts to get fairly small. Higher frequency *P/S* ratios (6 Hz and above) have become an important discriminant when they are available because of this apparent lack of material property dependence and good discrimination performance in all regions where good empirical data is available.

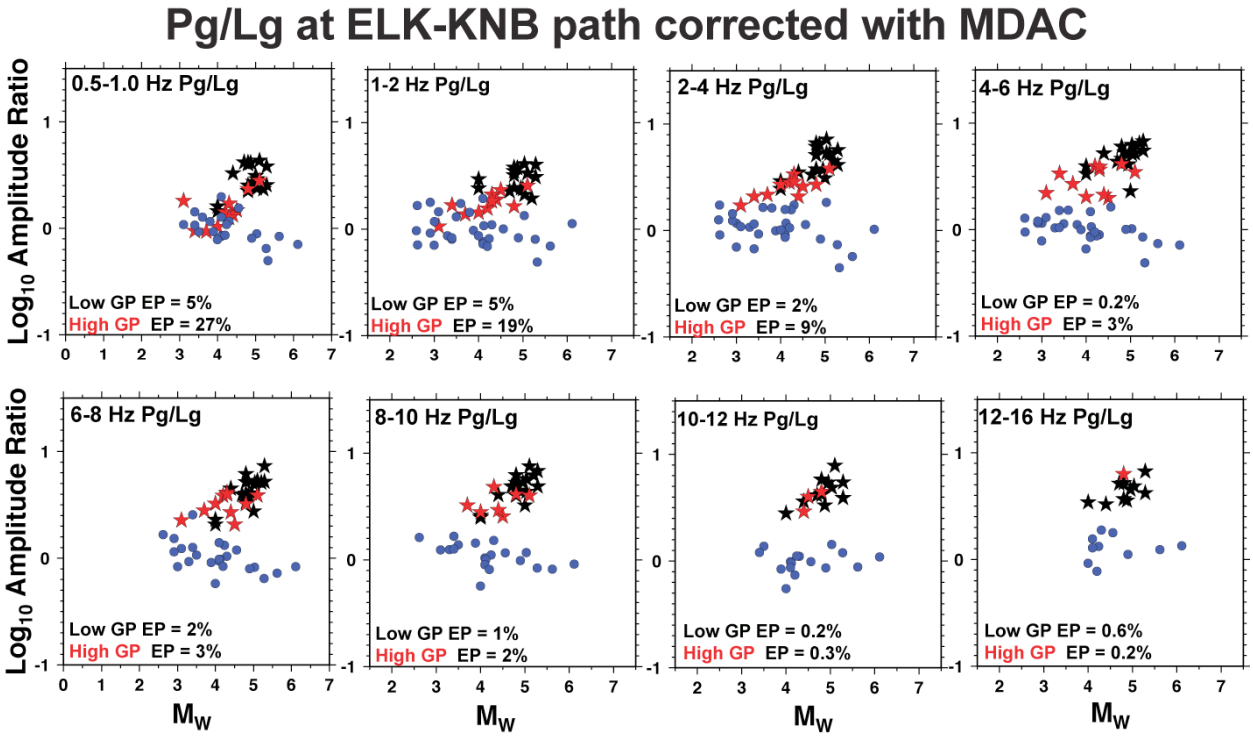

Figure 5. Pg/Lg ratios for two-station (ELK-KNB), averaged, MDAC-corrected, NTS-region data. We separate the nuclear explosions into high-strength/low-gas-porosity (black) and low-strength/high-gas-porosity (red) populations, as in Figure 4. There is some evidence of a material property effect at low frequencies, but not at frequencies above 6 Hz. Note that discrimination performance in general continues to improve as frequency increases, at least to 12 Hz, but the number of events passing the SNR decreases significantly.

Are Long-Period Complexities Reflected in Short-Period Discriminants?

A remarkable feature of the high frequency *P/S* ratios for discriminating underground nuclear tests is that they seem to work about as well in cases where the long-period signals indicate that the explosions are complex as in cases where the long-period signals are very simple. For example, if we contrast the May 11, 1998, Indian test with the October 9, 2006, North Korean test, both show good high-frequency *P/S* discrimination in Figure 2. However, the Indian test shows significant Love waves and reversed Rayleigh waves (Walter et al, unpublished data; Selby et al., unpublished data), indicating a large amount of tectonic release and significant non-isotropic components of the moment tensor source. On the other hand, waveform modeling of the North Korean test shows almost no Love waves and a nearly pure isotropic moment tensor (e.g., Walter et al, 2007). Despite the complexities in the Indian test source, the S-waves disappear at frequencies of 1 Hz and higher, and the test easily discriminates from nearby earthquakes, as shown in Figure 2 and by Rogers and Walter (2002).

To better understand any connections between complexities in the long period signal and the high frequency discriminants, we are making use of the waveform modeling results of Ford et al., 2008 (see also Ford et al., these

Proceedings). For example, it has been proposed that the explosions can have a significant compensated linear vector dipole (CLVD) component as part of their interaction with the free surface and that this can impact surface wave magnitude and perhaps S-wave amplitudes as well (Patton and Taylor, 2008). In Figure 6, we compare Pg/Lg ratios in two frequency bands to the relative CLVD strength from waveform modeling. At the 1- Hz band there may be a correlation that is not apparent at the high frequencies. However, we are still assessing just how well resolved the relative CLVD components from the waveform model are before reaching any conclusions. We hope to have updated results to present at the meeting. Finally, we note that there is clear evidence from the coda that the absolute depth of burial has an affect on Rg excitation (e.g., Murphy et al., 2008), and to the extent the Rg scatters into Lg, which can be significant (Myers, personal communication), this also affects the 1–2 Hz Pg/Lg ratios.

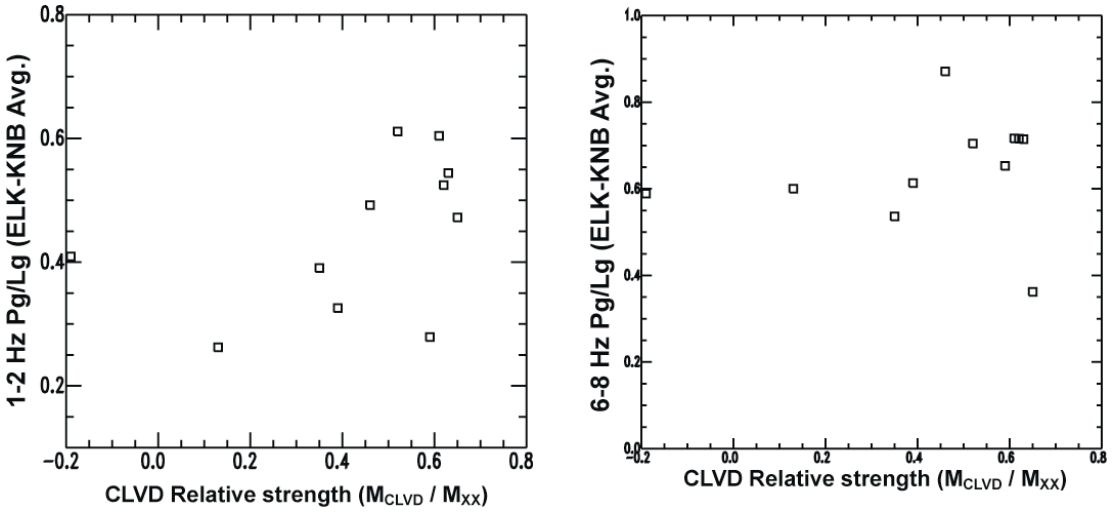

Figure 6. We compare 1–2 Hz and 6–8 Hz Pg/Lg ratios for NTS explosions averaged from ELK and KNB to the relative CLVD strength determined from waveform modeling (Ford et al., 2008). Note there appears to be a correlation for low frequency (excepting METROPOLIS, which has a negative CLVD relative strength) but not for high frequency. Coda-derived spectra show a peak tied to absolute depth (Murphy et al., 2008), which appears related to Rg excitation and independent of scaled depth of burial (and spall/CLVD). Low-frequency Lg thus appears to be affected by both absolute depth Rg effects and relative depth spall/CLVD effects.

Amplitude Tomography

In the MDAC corrections discussed so far, we have been using a single 1-D attenuation correction for a given station to a given region. However, it is well understood that in tectonically complex regions such as the Middle East, there can be very significant differences in the apparent attenuation of regional phase amplitudes over short distances. For example, Figure 7 shows a fairly dramatic example of large differences in the relative amplitude of 6-8 Hz Pn and Sn for two Zagros mountain events of about the same size and distance away. The top earthquake has the large Pn amplitude and weak Sn amplitude that we associate with explosions, particularly when compared with the other earthquake (e.g., Figure 1). To the extent these differences are due not to differences in source depth and mechanism but to propagation effects, we want to map them out and be able to correct for them. To do this, we are applying regional amplitude tomography techniques.

Crustal regional phase (Pg, Lg) amplitudes corrected for instrument and an assumed geometrical spreading (*A'*) can be written as a combination of source (S), path attenuation (R), and site (P) effects:

$$A'_{ij} = S_i * R_{ij} * P_j$$

Traditional amplitude tomographic techniques (e.g., Phillips and Stead, 2008) can then solve for each of these terms, with some tradeoffs between them. However, this results in source terms that can be significant. Given a new

event in a calibrated region, we want to be able to apply the tomographically derived apparent attenuation and get a predicted amplitude to use as a correction before forming a discriminant. What source term is associated with the new event? One way to make the source term more amenable for amplitude correction is to formulate it in terms of the MDAC (Walter and Taylor, 2001) modified Brune (1970) source term:

$$S_i = \frac{FM_o}{1+\frac{\omega^2}{\omega_c^2}} \quad where \quad \omega_c = \left(\frac{K\sigma}{M_o}\right)^{1/3}$$

where F and K are constants that depend on velocity, density, and average radiation patterns (see Walter and Taylor, 2001, for details), and where σ is the apparent stress in the region. In this case, the source term in the tomography can be reformulated to solve for the change in moment from the assumed initial moment, where the initial moment comes from a calibrated coda moment technique (e.g., Mayeda et al., 2003) or other technique (e.g., waveform modeling). In this case, for a new event, the moment is first determined and then a 2D attenuation MDAC correction applied to get the predicted amplitude for an earthquake of that Mw and location, much as we have been using the 1D path correction in the MDAC methodology.

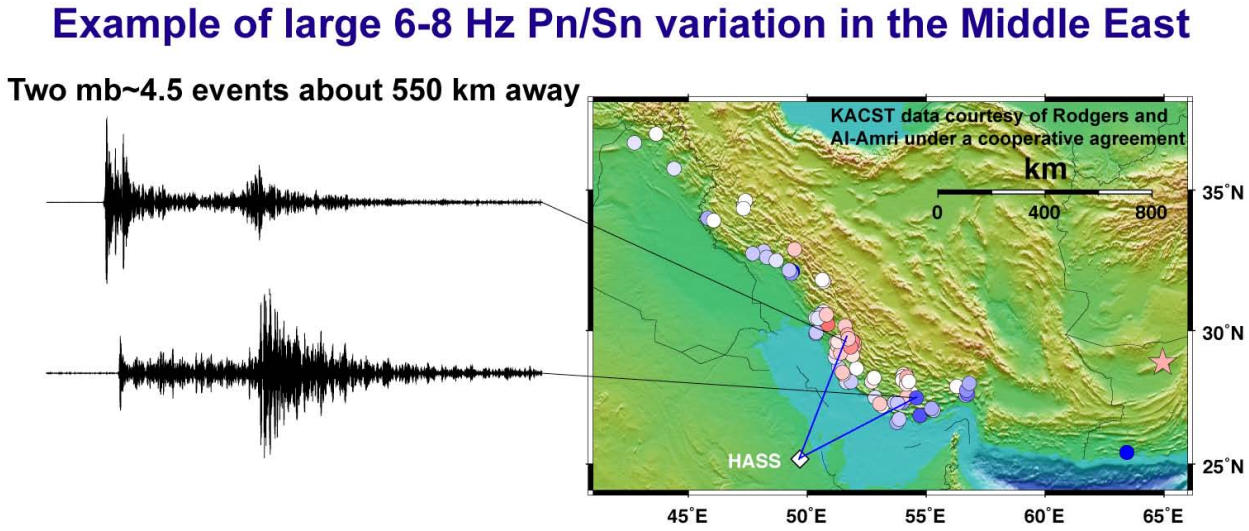

Figure 7. An example of large *P/S* ratio differences for two events of similar size and distance that appear to be due to complex path effects. Top event looks explosion-like relative to the bottom event. We are exploring amplitude tomographic techniques to account for and correct 2-D path effects on regional amplitudes used in discriminants.

Finally, if a good estimate of the source spectrum is available independently, through a coda technique or some other way, it is straightforward to use that for the source term directly and just solve for the path and site terms (e.g., Walter et al., 2007b). We are in the process of applying and testing these three variations of amplitude tomography in the Yellow Sea Korean Peninsula region (see Ford et al., these Proceedings) and in the Middle East. We plan to show some initial results at the meeting.

CONCLUSIONS AND RECOMMENDATIONS

Regional discrimination algorithms require calibration at each seismic station to be used for nuclear explosion monitoring. We apply MDAC procedures to remove source size and path effects from regional body-wave phases. This allows comparison of any new regional events recorded at a calibrated station with all available reference data and models. This also facilitates the combination of individual measures at multiple stations to form multivariate discriminants that can significantly improve performance over single-station individual measures. We are working to quantify the performance of *P/S* ratio discriminants as a function of a number of factors, including frequency, phase type, source media properties, long-period moment tensor, and 2-D apparent attenuation patterns.

ACKNOWLEDGEMENTS

We thank Stan Ruppert and Terri Hauk for loading and maintaining the Lawrence Livermore National Laboratory (LLNL) database. We thank Doug Dodge and Mike Ganzberger for developing and maintaining the LLNL software code RBAP, which was used to make the regional measurements. Regional phase-amplitude measurements were made using picks by the authors, as well as by former summer students Veronica Parker and Lindsay Lowe and by our expert analyst Ms. Flori Ryall.

REFERENCES

Battone, S., M. D. Fisk, and G. D. McCarter (2002), Regional Seismic-Event Characterization Using a Bayesian Formulation of Simple Kriging, *Bull. Seism. Soc. Am.* 92: 2277–2296.

Baumgardt, D. R. and G. B. Young (1990). Regional seismic waveform discriminants and case-based identification using regional arrays, *Bull. Seism. Soc. Am.* 80: 1874–1892.

Brune, J. (1970). Tectonic stress and the spectra from seismic shear waves earthquakes, *J. Geophys. Res*. 75: 4997–5009.

Dysart, P. S. and J. J. Pulli (1987). Spectral study of regional earthquakes and chemical explosions recorded at the NORES array. SAIC technical report C87-03.

Ford, S. R., D.S. Dreger, and W. R. Walter (2008). Identifying isotropic events using a regional moment tensor inversion, submitted to *J. Geophys. Res.*

Hartse, H., S. R. Taylor, W. S. Phillips, and G. E. Randall (1997). A preliminary study of regional seismic discrimination in Central Asia with an emphasis on Western China, *Bull. Seism. Soc. Am*. 87: 551–568.

Kim, W. –Y., D. W. Simpson, and P. G. Richards (1993). Discrimination of earthquakes and explosions in the eastern United States using regional high frequency data, *Geophys. Res. Lett.* 20: 1507–1510.

Mayeda, K., A. Hofstetter, J. O'Boyle and W. R. Walter (2003). Stable and Transportable Regional magnitudes based on coda derived moment-rate spectra, *Bull. Seism. Soc. Am*. 93: 224–239.

Murphy, K. R., K. Mayeda, and W. R. Walter (2008). Lg-coda methods applied to Nevada Test Site events: spectral peaking and yield estimation, submitted to *Bull. Seism. Soc. Am.*

Patton, H. J. and S. R. Taylor (2008). Effects of induced tensile failure on mb-Ms discrimination: contrasts between historic nuclear explosions and the North Korean test of 9 October 2006., *Geophys. Res. Lett.*, in press.

Phillips, W. S. and R. J. Stead (2008). Attenuation of Lg in the western U.S. using the USArray, *Geophys. Res. Lett.* 35: L07307, doi:10.1029/2007GL032926.

Rodgers, A. J. and W. R. Walter, (2002). Seismic Discrimination of the May 11, 1998 Indian Nuclear Test with Short-Period Regional Data From Station NIL (Nilore, Pakistan), *Pure Appl. Geophys.* 159: 679–700.

Springer, D. L., G. A. Pawlowski, J. L. Ricca, R. F. Rohrer, and D. K. Smith (2002). Seismic source summary for all U.S. below-surface nuclear explosions, *Bull. Seism. Soc. Am.* 92, 1806–1840.

Taylor, S., (1996). Analysis of high-frequency Pg/Lg ratios from NTS explosions and Western U.S. earthquakes, *Bull. Seism. Soc. Am.* 86: 1042–1053.

Taylor, S., A. Velasco, H. Hartse, W. S. Philips, W. R. Walter, and A. Rodgers, (2002). Amplitude corrections for regional discrimination, *Pure. App. Geophys*. 159: 623–650.

Walter, W. R., K. Mayeda, and H. J. Patton (1995). Phase and spectral ratio discrimination between NTS earthquakes and explosions Part 1: Empirical observations, *Bull. Seism. Soc. Am.*, 85: 1050–1067.

Walter, W. R. and S. R. Taylor (2001). A revised Magnitude and Distance Amplitude Correction (MDAC2) procedure for regional seismic discriminants, Lawrence Livermore National Laboratory UCRL-ID-146882: http://www.llnl.gov/tid/lof/documents/pdf/240563.pdf

Walter, W. R., E. Matzel, M. E. Pasyanos, D. B. Harris, R. Gok and S. R. Ford (2007a), Empirical observations of earthquake and explosion discrimination using *P/S* ratios and implications for the sources of explosion S-waves, in Proceedings of the 29th Monitoring Research Review: Ground-Based Nuclear Explosion Monitoring, LA-UR-07-5613, Vol. 1, pp. 684–693.

Walter, W. R., K. Mayeda, L. Malagnini, and L. Scognamiglio (2007b). Regional body-wave attenuation using a coda source normalization method: application to MEDNET records of earthquakes in Italy, *Geophys. Res. Lett.* 34: L10308, doi:10.1029/2007GL029990.